In vitro blood-brain-barrier permeability and cytotoxicity of atorvastatin-loaded nanoformulation against glioblastoma in 2D and 3D models

Michael M. Lübtow[1], Sabrina Oerter[2], Sabina Quader[3], Elisabeth Jeanclos[4,5], Alevtina Cubukova[6], Marion Krafft[2], Malik Salman Haider[1], Clemens Schulte[1], Laura Meier[1], Maximilian Rist[1], Oltea Sampetrean[7], Hiroaki Kinoh[3], Antje Gohla[4], Kazunori Kataoka[3,8], Antje Appelt-Menzel[2,6], Robert Luxenhofer[1,9*]

[1] *Functional Polymer Materials, Chair for Advanced Materials Synthesis, Department of Chemistry and Pharmacy and Bavarian Polymer Institute, University of Würzburg, Röntgenring 11, 97070 Würzburg, Germany*

[2] *University Hospital Würzburg, Chair Tissue Engineering and Regenerative Medicine (TERM), Röntgenring 11, 97070 Würzburg, Germany*

[3] *Innovation Center of Nanomedicine (iCONM), Kawasaki Institute of Industrial Promotion, 3-25-14 Tonomachi, Kawasaki-Ku, Kawasaki-Shi 210-0821, Japan*

[4] *Institute of Pharmacology and Toxicology, University of Würzburg, Versbacher Straße 9, 97078 Würzburg, Germany*

[5] *Rudolf Virchow Center for Experimental Biomedicine, University of Würzburg, Josef-Schneider-Straße 2, 97080 Würzburg, Germany*

[6] *Fraunhofer Institute for Silicate Research ISC, Translational Center Regenerative Therapies TLC-RT, Röntgenring 11, 97070 Würzburg, Germany*

[7] *Institute for Advanced Medical Research (IAMR), Division of Gene Regulation, Keio University School of Medicine, 35 Shinanomachi, Shinjuku-ku, Tokyo, 160-8582, Japan*

[8] *Policy Alternatives Research Institute, The University of Tokyo, 7-3-1 Hongo, Bunkyo-ku, Tokyo, 113-0033 Japan*

[9] *Soft Matter Chemistry, Department of Chemistry, Helsinki University, 00014 Helsinki, Finland*

correspondence to: robert.luxenhofer@uni-wuerzburg.de

Keywords

drug-loaded micelles, poly(2-oxazoline), poly(2-oxazine), nanomedicine, human induced-pluripotent stem cells, cancer stem cells

ABSTRACT: Inhibitors of 3-hydroxy-3-methylglutaryl-coenzyme A (HMG-CoA) reductase of the family of statins have been suggested as therapeutic options in various tumors. Atorvastatin is a statin with potential to cross the blood-brain-barrier, however, the concentrations necessary for a cytotoxic effect against cancer cells exceeds the concentration achievable via oral administration, which made the development of a novel atorvastatin formulation necessary. We characterized the drug loading and basic physicochemical characteristics of micellar atorvastatin formulations and tested their cytotoxicity against a panel of different glioblastoma cell lines. In addition, activity against tumor spheroids formed from mouse glioma and mouse cancer stem cells, respectively, was evaluated. Our results show good activity of atorvastatin against all tested cell lines. Interestingly, in the 3D models, growth inhibition was more pronounced for the micellar formulation compared to free atorvastatin. Finally, atorvastatin penetration across a blood-brain-barrier model obtained from human induced-pluripotent stem cells was evaluated. Our results suggest that the presented micelles may enable much higher serum concentrations than possible by oral administration, however, if transport across the blood-brain-barrier is sufficient to reach therapeutic atorvastatin concentration for the treatment of glioblastoma via intravenous administration remains unclear.

1. INTRODUCTION

Glioblastoma (GBM) is the most common and most aggressive cancer of the central nervous system exhibiting dismal 5-year survival rates of 5 %.[1-2] Currently, surgical resection (limited due to diffuse and infiltrative nature of GBM) and concomitant chemoradiotherapy offer highest median survival rates of 14 months.[3] Chemotherapy of GBM is especially challenging due to the rapid proliferative rate of GBM cells[4], the appearance of treatment resistant cell clones shortly after initial treatment[5-6] as well as the limited access of systemically administered agents to the brain parenchyma due to the blood-brain-barrier (BBB)[7-8]. Despite these drawbacks, chemoradiotherapy greatly improves mean 3-year survival rates from 1.9 to 16 % compared to radiotherapy alone in the case of the most widely used chemotherapeutic agent for GBM treatment, temozolomide (TMZ).[3] However, rapid development of TMZ resistance underline the urgent clinical need for better treatment options, potentially by using alternative active pharmaceutical ingredients (APIs) for GBM chemotherapy.[9]

Statins are a family of widely used drugs for the treatment of hypercholesterolemia.[10] They act as inhibitors of 3-hydroxy-3-methylglutaryl-coenzyme A (HMG-CoA) reductase thus being potent inhibitors of cholesterol biosynthesis.[11] However, beyond their effects on serum cholesterol levels, recent research effort gives increasing evidence on cancer prevention and/or treatment properties of statins through interactions with essential cellular functions such as cell proliferation and differentiation.[12] Several *in*

vitro and *in vivo* studies have demonstrated tumor growth inhibition as well as induction of apoptosis in various melanoma[13], glioma[14], neuroblastoma[15], leukemia[16] as well as glioblastoma cell lines[17]. The underlying modes of action of statins causing (i) inhibition of tumor cell growth, (ii) repression of tumor metastases, (iii) inhibition of angiogenesis and (iv) induction of apoptosis were comprehensively reviewed by Hindler *et al*.[12], Pisanti *et al*.[18] and Gizzo *et al*.[19]

As cell replication of GBM is highly dependent on the mevalonate (MVA) pathway for the synthesis of lipid moieties, their growth is naturally highly vulnerable to statins acting as competitive inhibitors of the enzyme regulating MVA synthesis – HMG-CoA reductase.[20-21] Furthermore, lovastatin increases the expression of the peroxisome proliferator-activated receptor, a transcription factor implicated in the control of lipid metabolism, cell growth and differentiation thus strongly reducing glioma proliferation.[20] Real-time PCR analysis of U87 glioma spheroids revealed that atorvastatin (ATV) induced cell apoptosis by down-regulating the expression of anti-apoptotic Bcl-2 and up-regulating apoptotic caspase-3 and caspase-8 factors.[22] Increase in caspase-3 activity in glioblastoma was also confirmed for other statins.[17] Investigating the Ras downstream cascade, it was found that the increase was due to a reduced phosphorylation of extracellular signal-regulated kinase 1/2 (ERK1/2) and Akt. As the activation levels of these signal transduction molecules were restored in the presence of geranylgeranyl-pyrophosphate (GGPP), the inhibition of ERK1/2 and Akt activation in C6 glioma cells was correlated to the inhibition of GGPP biosynthesis.[17] ATV also reduced the pro-tumorigenic effects of microglia on glioma migration and invasion by reducing the microglial expression of membrane type 1 metalloproteinase (MT1-MMP).[23] It was suggested that the down-regulation of MT1-MMP was controlled by a p38 MAPK pathway in microglia. Furthermore, ATV was suggested to decrease the expression of pro-inflammatory proteins and interleukins (IL).[24] This is important, as inflammatory microenvironment generally promotes malignant progression[25] which is especially true for GBM[26]. Although not discussed in direct correlation with GBM but worth mentioning, statins have been reported to sensitize cells to ferroptosis and induce ferroptosis in selected cell lines (however, further studies are necessary to confirm this).[27] Furthermore, combination therapy of temozolomide and ATV in combination with radiotherapy in newly diagnosed GBM patients was promising (progression free survival (PFS) rate at 6 months: 67 % and median PFS of 9.1 months), meeting criteria for continued accrual in a phase II clinical study (NCT02029573).[28] In addition, considerable evidence suggests that statins also exhibit immunomodulatory properties,[18] as e.g. the number and suppressive function of regulatory T cells was decreased by ATV in patients with rheumatoid arthritis.[29]

Although both, hydrophilic and lipophilic statins demonstrated antitumor effects, hydrophobic APIs generally exhibit a higher permeability through the BBB by e.g. passive diffusion.[30] However, lipophilic substances also tend to be substrates for P-glycoprotein, potentially reversing this effect[31-32]. That this general trend is also true for statins was confirmed by Tsuji *et al*.[33], observing permeation of lipophilic lovastatin and simvastatin but not of hydrophilic pravastatin through an artificial BBB *in vitro*, later this was also confirmed *in vivo*[34]. Important to note, among various statins, ATV is the most frequently reported one for causing adverse neurocognitive effects compared to less lipophilic statins which was associated with its increased permeability through the BBB.[35-36] Therefore, we chose lipophilic ATV as potential cytotoxic API against various glioblastoma cell lines.

However, besides the issue of passing the BBB, transportation of APIs to the BBB at sufficient high drug concentration is crucial. This can be especially challenging for hydrophobic APIs such as ATV which cannot simply be administered e.g. intravenously and oral bioavailability may not be sufficient to achieve concentrations necessary to reliably exhibit anti-tumor activity. Nanomedicine offers great potential regarding intravenous administration of water-insoluble drugs.[37-38] A few ATV-loaded polymer micelles based on amphiphilic polylactic acid-*b*-PEG-*b*-polylactic acid (PLA-PEG-PLA) triblock copolymers[39], PEG-poly(ε-caprolactone) (PEG-PCL) diblock copolymers[40], PEG-*b*-vitamin E succinate (PEG-VES)[41], stearyl grafted chitosan (SC)[42] or ATV-loaded bovine serum albumin (BSA) nanoparticles[43] can be found in the literature. However, to the best of our knowledge, none of these systems was investigated with respect to GBM treatment. Interestingly though, polysorbate 80 coated, ATV-loaded poly(lactic-*co*-glycolic acid)-*b*-PEG (PLGA-PEG) nanoparticles have been designed to investigate the influence of the coating on the transport of ATV to the brain.[44] Important to note, both – coated and uncoated nanoparticles – were able to penetrate the BBB *in vivo* reaching maximum brain-concentration 1 h post-intravenous injection. Pioneering work by Kabanov and co-workers revealed that several amphiphilic polymers can facilitate transport of small molecules and proteins across the BBB.[45-48] In addition, Zentel and co-workers could show that also am-phiphilic copolymers based on 2-hydropropylacrylamide and laurylacrylate could increase transport of small molecules across the BBB *in vitro* and *in vivo*.[49-51]

2. MATERIALS AND METHODS

Reagents and Solvents

The monomers 2-*n*-propyl-2-oxazoline (PrOx), 2-*n*-propyl-2-oxazine (PrOzi), 2-*n*-butyl-2-oxazoline (BuOx) and 2-*n*-butyl-2-oxazine (BuOzi) were synthesized according to Seeliger *et al*.[52] as reported recently[53]. The polymers **A-pPrOx-A** (Me-MeOx$_{36}$-PrOx$_{20}$-MeOx$_{36}$-1-Boc-piperazine (PipBoc)), **A-pBuOx-A** (Me-MeOx$_{35}$-BuOx$_{20}$-MeOx$_{35}$-piperidine), **A-pPrOzi-A** (Me-MeOx$_{35}$-PrOzi$_{20}$-MeOx$_{35}$-PipBoc) and **A-pBuOzi-A** (Prop-MeOx$_{35}$-BuOzi$_{20}$-MeOx$_{35}$-PipBoc) were synthesized recently.[53] Pluronic® was a mixture of Pluronic® F127 and L61 at 8/1 (w/w) corresponding to the ratio reported for SP1049C®. Atorvastatin (calcium salt trihydrate) was purchased from *Sigma-Aldrich* (HPLC ≥ 98 %). Deuterated chloroform ($CDCl_3$), dimethyl sulfoxide (DMSO-d_6) or water (D_2O) for ^{1}H-NMR analysis were obtained from *Deutero GmbH* (Kastellaun, Germany).

Experiments

Nuclear Magnetic Resonance Spectroscopy (NMR)

NMR spectra were recorded on a Fourier 300 (300 MHz), *Bruker Biospin* (Rheinstetten, Germany) at 298 K. The spectra were calibrated to the signal of residual protonated solvent signal ($CDCl_3$: 7.26 ppm; DMSO-d_6: 2.50 ppm, D_2O: 4.79 ppm).

ATV-loaded Polymer Micelles

ATV-loaded polymer micelles were prepared by thin film method.[54] Methanolic polymer (20 g/L) and ATV (20 g/L) stock solutions were mixed in desired ratio. After complete removal of the solvent at 40 °C under a mild stream of argon, the films were dried *in vacuo* (≤ 0.2 mbar) for 20 min. Subsequently, H_2O was added. Complete solubilization was facilitated by shaking the solutions at

1250 rpm at 35 °C for 12 min with a Thermomixer comfort, *Eppendorf AG* (Hamburg, Germany). Non-solubilized drug (if any) was removed by centrifugation for 5 min at 9.000 rpm with a MIKRO 185 (*Hettich,* Tuttlingen, Germany). Solubilization experiments were performed with 3 individually prepared samples and results are presented as mean ± standard deviation (SD).

ATV Quantification by HPLC

ATV quantification was performed by HPLC on a LC-20A Prominence HPLC, *Shimadzu* (Duisburg, Germany) equipped with a system controller CBM-20A, a solvent delivery unit LC-20 AT (double plunger), an on-line degassing unit DGU-20A, an auto-sampler SIL-20AC, and a SPD-20A UV-Vis detector. As stationary phase, a ZORBAX Eclipse Plus, *Agilent* (Santa Clara, CA, USA) C18 column (4.6 x 100 mm; 3.5 µm) was used. The mobile phase was a gradient of H_2O/ACN (60 % - 40 % H_2O; Figure S1a) at 40 °C and a flow rate of 1 mL/min. Prior to ATV quantification, all formulations were centrifuged to remove any precipitate, diluted with ACN/H_2O = 60/40 (v/v) and quantified at 245 nm (Figure S1b). The following equations were used to calculate loading capacity (*LC*) and loading efficiency (*LE*):

$$LC = \frac{m_{drug}}{m_{drug} + m_{polymer}} \quad (1)$$

$$LE = \frac{m_{drug}}{m_{drug,added}} \quad (2)$$

where m_{drug} and $m_{polymer}$ are the weight amounts of solubilized drug and polymer excipient in solution and $m_{drug,added}$ is the weight amount of drug initially added to the dispersion. No loss of polymer during micelle preparation was assumed.

Long-term Stability Studies

For long-term stability studies, ATV-loaded polymer micelles were stored in Eppendorf tubes containing the precipitate (if any occurred) at ambient conditions (≈ 25 °C) under the exclusion of light. Prior to ATV quantification, all formulations were centrifuged to remove any precipitate, diluted with ACN/H_2O = 60/40 (v/v) and quantified by HPLC analysis at 245 nm.

Dynamic Light Scattering (DLS)

DLS measurements were performed on a Zetasizer Nano ZS (*Malvern Panalytical GmbH*, Kassel, Germany) with a 633 nm HeNe-laser at 173°. Autocorrelations for each sample were obtained 3 times for 40 seconds and results are presented as mean. Prior to the measurements, all samples (polymer = 10 g/L) were diluted 1/5 (v/v) with ultrapure H_2O to polymer = 2 g/L. The samples were measured unfiltered in quartz cuvettes (d = 10 mm, QS, *Hellma*) at 25 °C.

2D Cell Viability and Migration Studies

Mouse glioma cells (CT-2A and GL261) as well as human glioblastoma cells U373, U251 and U87 were cultured in Dulbecco's Modified Eagle's medium (DMEM; *Sigma-Aldrich*, St. Louis, USA) (high glucose) supplemented with 10 % fetal bovine serum (FBS). In the case of CT-2A, U373 and GL261, 1 % penicillin/streptomycin (P/S) was added. For U373, Gibco® MEM non-essential amino acids were added as well. For the determination of IC_{50}, cells were seeded at 3 x 10^3 cells/well in transparent flat-bottom 96 well-plates and cultured for 1 d in humidified atmosphere of 5 % CO_2 at 37 °C. DMSO/ATV was prepared by dissolving 10 g/L ATV in DMSO and diluted with D-PBS(-) (PBS = phosphate buffered saline, *FUJIFILM Wako Pure Chemicals* Corporation (Osaka, Japan) to 1 g/L ATV before further dilution with cell specific medium to desired ATV concentrations. ATV-loaded **A-pBuOzi-A** micelles were prepared by thin-film method (ρ(**A-pBuOzi-A**/ATV) = 10/1 [g/L]) and diluted with cell-specific medium to desired ATV concentrations. The respective solutions were applied for 24 h, 48 h and 72 h. After treatment, Cell Counting Kit-8 (CCK8) cell proliferation/cytotoxicity assay was performed according to manufacturer's instructions. Briefly, 10 µL of CCK-8 solution were added per well and the samples incubated for 2 h at 37 °C and 5 % CO_2. Absorption was measured at λ_{abs} = 450 nm with an Infinite 200 (Tecan, Männedorf, Switzerland).

Cell viability was determined by equation 3:

$$cell\ viability = \frac{F_{treated} - F_{medium}}{F_{untreated} - F_{medium}} x\ 100\ \% \quad (4)$$

where $F_{treated}$ and $F_{untreated}$ correspond to the absorption of treated and untreated cells, respectively, and F_{medium} is the absorption of the culture medium.

Cell viability experiments were performed with three individual 96 well-plates containing each sample concentration in quadruplicate and results are presented as means ± SD. IC_{50} was determined with OriginPro 2019 software using a Boltzmann or biphasic dose-response fit.

Human pediatric cerebellar glioblastoma multiforme GBM6840 cells were cultured in DMEM (high glucose) supplemented with 10 % FBS. Cell viability studies and IC_{50} determinations were conducted by live/dead cell staining and flow cytometric analysis. Briefly, cells were seeded in 96 well-plates (10^4 cells/well). The next day, ATV (solubilized in DMSO or formulated with **A-pBuOzi-A**) was added to the medium at a final concentration of 0 to 80 µM. The corresponding concentrations of DMSO and **A-pBuOzi-A** alone served as controls. After 48 h incubation, cells were rinsed with PBS, trypsinized, and resuspended in 250 µL PBS containing 0.5 g/L soybean trypsin inhibitor (*Invitrogen*, Carlsbad, USA). Cell culture medium, wash solution and trypsinized cells were collected and incubated for 15 min at 22 °C with the live cell indicator calcein-AM *(Invitrogen*, Carlsbad, USA) at a final concentration of 10 nM. Immediately before flow cytometry, cell suspensions were incubated with the dead cell indicator propidium iodide (1 mg/L, *Invitrogen*) for 1 min. Cells were analyzed on a FACS Calibur flow cytometer (*Beckton Dickinson*, Heidelberg, Germany); at least 5,000 cells were analyzed per condition. Data are presented as means ± SEM of *n*=3 independent experiments. Cell viability was expressed as the percentage of calcein-positive cells. IC_{50} values were determined by non-linear regression (log(inhibitor) vs. response – variable slope (four parameters)) using Prism v7.04 (*GraphPad*, San Diego, U.S.A.).

For cell migration studies, 2 x 10^5 GBM6840 cells were seeded in 3 cm dishes and treated with 0, 2.5 or 5 µM ATV formulated with **A-pBuOzi-A** for 65 h. GBM6840 cells were trypsinized, resuspended in 1 mL DMEM containing 0.5 mg/mL soybean trypsin inhibitor, and washed once by centrifugation (300 × *g*, 5 min at RT). The cell suspension (2.5 x 10^4 cells/0.5 mL DMEM) was added to the upper compartment of a transwell (Falcon cell culture inserts for 24 well-plates, 8 µm pore size; *ThermoFisher Scientific*). The bottom side of the membrane was pre-coated with fibronectin (10 mg/mL; *Sigma-Aldrich*) to assure attachment of the transmigrated cells; epidermal growth factor (100 ng/mL; *Sigma-Aldrich*) was used as a chemoattractant in the lower transwell compartment. Cells were allowed to migrate for 8 h in a humidified tissue culture

incubator (37 °C, 5 % CO_2) in the presence of 0, 2.5 or 5 µM ATV. Remaining cells on the upper side of the transwell membranes were removed with cotton swabs, and cells on the lower side of the membranes were fixed with 4 % (w/v) para-formaldehyde for 20 min. Nuclei were stained with 4',6-diamidine-2'-phenylindole (DAPI, 1 µg/mL) in PBS, and transwells were mounted on coverslips using Immunomount (*ThermoFisher Scientific*). Cell nuclei were visualized on a Leica SP5 confocal microscope (*Leica Microsystems*) equipped with a 10× objective, and four images covering ≈ 75 % of the total transwell membrane surface area were taken for each transwell. Cell numbers were quantified semi-automatically using ImagePro-Plus software, version 7.0 (*Media Cybernetics*, Rockville, U.S.A.).

3D Spheroid studies

CT-2A cells were cultured in DMEM supplemented with 10 % FBS and 1 % P/S. Mouse brain tumor initiating bRiTS-G2 cells were cultured in DMEM/F12 (*Wako*, Osaka, Japan) supplemented with 20 ng/mL epidermal growth factor, 20 ng/mL basic fibroblast growth factor (both *PeproTech*, Rocky Hill, NJ), B27 supplement without vitamin A (*Invitrogen*, Carlsbad, USA) and 200 ng/mL heparan sulfate (*Sigma-Aldrich*, St. Louis, USA). For spheroid studies, cells were seeded at 5 x 10^3 cells/well in all white U-bottom 96 well-plates (PrimeSurface96U, *Sumitomo Bakelite Co*. Tokyo, Japan) and incubated for 1 d in humidified atmosphere of 5 % CO_2 at 37 °C. Within this time, 3D cell aggregates of around 400 µm diameter were spontaneously formed (Figure S2). Subsequently, stock solutions of **A-pBuOzi-A**/ATV (ρ(**A-pBuOzi-A**/ATV) = 10/1 [g/L] in ultrapure H_2O) or DMSO/ATV (ATV = 10 g/L) were diluted with cell specific culture medium to desired concentrations and applied for 48 h and 72 h. After treatment, CellTiter-Glo® 3D Luminescent Cell Viability Assay (*Promega*, Madison, USA) was performed according to manufacturer's instructions. Briefly, 100 µL of CellTiterGlo® 3D solution were added per well (100 µL) and stored for 30 min at ambient conditions (≈ 25 °C) under the exclusion of light. Luminescence was measured with a GloMax®-Multi+ Detection System (*Promega*, Madison, USA). Spheroid studies were performed with three individual 96 well-plates containing each sample concentration in quadruplicate and results are presented as means ± SD.

2D human iPSC-BBB Studies

Human induced-pluripotent stem cells (hiPSC; IMR90-4, *WiCell Research Institute*, USA) were cultured in mTeSR™1 medium (*StemCell Technologies*, Canada). The iPSC-derived BBB model was built as previously described.[55] Cytotoxicity of **A-pBuOzi-A**/ATV or DMSO/ATV against hiPSC-derived endothelial cells (hiPS-ECs) was evaluated for three concentrations (45 µM, 90 µM and 150 µM) after 4 h and 24 h incubation. After treatment, CellTiter-Glo® 3D Luminescent Cell Viability Assay (*Promega*, Mannheim, Germany) was performed according to manufacturer's instructions. Luminescence was measured with an Infinite M200 fluorescence reader (*Tecan Group*, Switzerland). Cytotoxicity studies were performed in triplicates and three independent biological replicates and results are presented as means ± SEM.

To evaluate human BBB-like characteristic, transendothelial electrical resistances (TEER) were determined with a Millicell ERS-2 voltohmmeter (*Millipore*, USA) equipped with a STX3 electrode (*World Precision Instruments*, Germany) prior transport assay. TEER measurements were performed 40 min after medium change. Each model was measured three times, monitoring and excluding a possible data drift due to temperature fluctuations and duplicates were used for each experiment in three independent biological replicates. To yield the TEER values [Ω*cm^2] resulted from BBB hiPS-ECs, average TEER of empty inserts coated with collagen IV/fibronectin were subtracted and values were multiplied by insert surface. Results are presented as means ± SEM.

Permeation through BBB endothelium

Transport assays were performed in transwells (24-well format) on an orbital shaker (*Edmund Bühler GmbH*, Germany) at 100 rpm, 37 °C, 95 % humidity, and 5 % CO_2. Stock solutions of **A-pBuOzi-A**/ATV or DMSO/ATV were diluted with human endothelial-SFM (*Thermo Fisher Scientific,* USA) containing 1 % platelet poor-plasma derived serum (PPPDS; *Alfa Aesar,* USA) to the desired concentrations ([ATV] = 90 µM and 150 µM). Test concentrations of **A-pBuOzi-A**/ATV or DMSO/ATV (200 µL) were applied to the apical side of the BBB model. The basolateral side was supplied with 800 µL of human endothelial-SFM containing 1 % PPPDS and the respective concentration of sterile water (**A-pBuOzi-A**) or DMSO. The permeation was evaluated after incubation times of 4 h and 24 h. Apical and basolateral media were analyzed by HPLC to quantify the transport of **A-pBuOzi-A**/ATV or DMSO/ATV. As control, the substances were incubated on empty collagen IV-/fibronectin-coated inserts to exclude major ATV adsorption on the membrane. All permeability studies were performed in duplicates and three independent biological replicates, results are presented as means ± SD. The level of statistical significance was set at $p<0.05$, indicated with asterisk (*). Grading in significance is indicated as follows: *$p<0.05$, **$p<0.01$, ***$p<0.001$.

3. RESULTS AND DISCUSSION

ATV solubilization

As reported recently, poly(2-oxazoline) (POx) and poly(2-oxazine) (POzi) based ABA triblock copolymers, all comprising the same hydrophilic poly(2-methyl-2-oxazoline) (PMeOx) shell **A** and structurally very similar, hydrophobic cores **B** exhibit different loading capacities for various hydrophobic drugs[53, 56-60] as well as varying drug/polymer interactions in dependence of the drug-loading[61-62]. Whereas the triblock copolymer with a barely hydrophobic poly(2-*n*-butyl-2-oxazoline) (pBuOx, = **A-pBuOx-A**) core enabled moderately high loadings of 24 wt.% of the hydrophobic compound curcumin (CUR), its structural isomer with a poly(2-*n*-propyl-2-oxazine) (pPrOzi; = **A-pPrOzi-A**) core was able to yield exceptionally high loadings up to 54 wt.%.[56] Interestingly, in the case of hydrophobic paclitaxel (PTX), the situation was *vice versa*, **A-pBuOx-A** being the best performer with PTX loadings up to 48 wt.% compared to 25 wt.% in the case of **A-pPrOzi-A**. As the drug loading is a crucial parameter concerning the translation of drug-loaded polymer micelles into the clinics, we investigated both polymers with regard to their solubilization capacity for the non-water soluble drug atorvastatin (ATV; water solubility of ATV calcium salt trihydrate by thin film-method = 60 mg/L (0.1 mM); analyzed in house). Additionally, two polymers comprising either a poly(2-*n*-propyl-2-oxazoline) (pPrOx; = **A-pPrOx-A**) or poly(2-*n*-butyl-2-oxazine) (pBuOzi; = **A-pBuOzi-A**) core were investigated for solubilization. The mixture of two Pluronics® SP1049C, which was developed by Kabanov for the interference with P-glycoprotein (P-gp) and therefore, improved delivery of hydrophobic molecules across biological barriers such as the BBB overexpressing P-gp[63-65] was included for comparison (Figure 1a). As expected, distinct polymer-ATV solubilization specificities were observed for the formulations pre-

pared by thin film method (Figure 1b). Whereas **A-pPrOx-A** enabled ATV concentrations of only 0.7 g/L (*LC* = 6.4 wt.%; ATV-feed = 10 g/L), its POzi counterpart with the same propyl-side chain **A-pPrOzi-A** solubilized up to 4.2 g/L ATV (*LC* = 29 wt.%; ATV feed = 10 g/L), being outperformed only by **A-pBuOzi-A** with up to 6.9 g/L ATV (*LC* = 41 wt.%; ATV feed = 10 g/L) (Figure 1c). Again, the POx with the same side chain **A-pBuOx-A** exhibited lower *LC*s of up to 25 wt.% (3.3 g/L; ATV feed = 10 g/L). The *LC* of Pluronic® was 6 times lower with ATV = 0.7 g/L (*LC* = 6.4 wt.% ATV-feed = 10 g/L), showing the same *LC* as **A-pPrOx-A**. As **A-pBuOzi-A** also exhibited the best long-term stability showing only minor loss in ATV-content up to ATV feed concentrations of 5 g/L within 30 d storage (Figure 1d; for 30 d long-term stability of all other formulations, please see Figure S3) this carrier was deemed most promising for further studies. Therefore, the physicochemical properties of **A-pBuOzi-A**/ATV formulations were investigated in more detail.

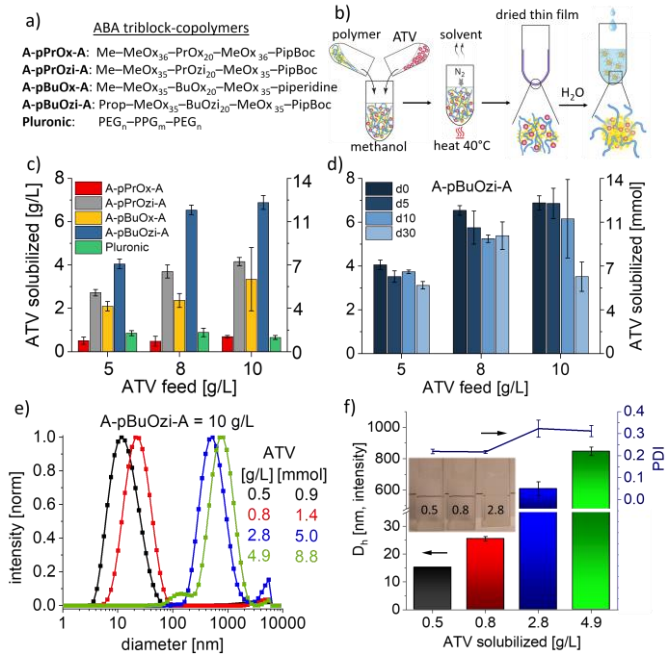

Figure 1: a) ABA triblock-copolymers used for ATV solubilization by b) thin-film method; c) solubilized aqueous ATV concentrations in dependence of the ATV feed by **A-pPrOx-A**, **A-pPrOzi-A**, **A-pBuOx-A**, **A-pBuOzi-A** or Pluronic® F127/L61 8/1 (w/w) at polymer = 10 g/L.; d) Long-term stability of **A-pBuOzi-A**/ATV formulations. Formulations were stored in Eppendorf-tubes containing the initial precipitate at ambient conditions (T ≈ 25 °C) under the exclusion of light. All formulations were prepared in triplicates and results are presented as means ± SD; e) particle size distribution determined by dynamic light scattering of **A-pBuOzi-A**/ATV formulations in dependence of the solubilized ATV concentration at room temperature (≈ 25 °C) at 173° with a Zetasizer Nano ZS. The samples (**A-pBuOzi-A** = 10 g/L) were diluted with H_2O 1/5 (v/v) and measured unfiltered; f) mean hydrodynamic diameter D_h (intensity weighted) of the ATV-loaded **A-pBuOzi-A** micelles. Each formulation was prepared three times and data is given as mean ± SD (n = 3). Inset in figure f) shows visual appearance of undiluted **A-pBuOzi-A**/ATV = 10/0.5; 10/0.8 and 10/2.8 g/L formulations.

Particle sizes of the **A-pBuOzi-A**/ATV formulations were highly dependent on the ATV-loading. At rather low loadings of 0.5 and 0.9 g/L (polymer = 10 g/L), micelles with average hydrodynamic diameters D_h of 15 nm and 26 nm were found, respectively (Figure 1e). The size distributions were monomodal with corresponding PDIs of 0.22 (Figure 1f). Increasing the ATV-loading to 2.8 and 4.0 g/L resulted in a dramatic increase in particle size to 609 nm and 847 nm, respectively, accompanied by an increase in PDI to 0.31 – 0.32. The increase in size was also apparent by visual inspection of the formulations (inset Figure 1f). Whereas up to **A-pBuOzi-A**/ATV = 10/0.8 g/L the formulations were completely clear, the sample containing 2.8 g/L ATV was opaque and emulsion-like (however samples for DLS were diluted 1/5 (v/v) to suppress artefacts due to multiple scattering etc.). Although being opaque, the samples did not show precipitation over extended periods of time (determined by visual inspection as well as relatively constant ATV loading up to 30 d (ATV feed = 5 & 8 g/L) or 10 d (ATV feed = 10 g/L) storage (Figure 1d)). A more detailed analysis of these aggregates using, *inter alia*, small angle neutron scattering is ongoing. However, such large aggregates, irrespective of their nature or structure are probably not ideal for the envisioned application *i.v.* for which smaller and better-defined micelles are preferred.

To get more insights into the ATV formulations on a molecular level[62], ^{1}H-NMR spectra of neat ATV, neat polymer or ATV formulations at varying **A-pBuOzi-A**/ATV ratio were recorded. In DMSO-d_6, all signals related to ATV were clearly visible with expected intensities (Figure 2; black spectrum; for enlarged ATV and **A-pBuOzi-A** spectra, the reader is referred to Figure S4 and S5, respectively). In contrast, when solubilized with **A-pBuOzi-A**, ^{1}H-NMR signals of ATV were either strongly attenuated and broadened (**A-pBuOzi-A**/ATV ≤ 10/0.9) or could not be detected anymore (**A-pBuOzi-A**/ATV > 10/0.9) in D_2O (Figure 2; enlarged spectra). A similar disappearance of ^{1}H-NMR signals was already observed for **A-pPrOzi-A**/CUR formulations.[66] Systems which are hindered in their mobility are predestinated for short transverse relaxation times T_2 causing a broadening or complete disappearance of certain signals. Therefore, the disappearance of the ^{1}H-NMR signals indicates a strong decrease in molecular mobility of ATV incorporated into the hydrophobic core of **A-pBuOzi-A** even at low loading. Furthermore, the signals of the butyl sidechain of the hydrophobic block are clearly affected (Figure 2 III-V). Notably, the signal attributed to the methyl group in the sidechain of pBuOzi (signal V) splits up. Besides the initial triplet, a second, much broader signal was observed at lower chemical shift. Similarly, but somewhat less pronounced, signals III and IV shift and became increasingly attenuated with increasing ATV loading. This decrease again is intuitive for a hindered mobility due to interactions of ATV with the hydrophobic block of **A-pBuOzi-A**. In contrast, the signals related to the hydrophilic shell (Figure 2 I,II) appear entirely unaffected even at the highest investigated drug loading. This results in a decreased ratio of the integrals of the methyl group of pBuOzi (core, signal V) with respect to the methyl sidechain of pMeOx (shell, signal II) with increasing ATV-loading (Figure S6). The more or less linear decrease of the ratio as well as the largely unaffected signals related to the hydrophilic shell are somehow surprising considering the large change in particle size at higher ATV-loadings observed by DLS (Figure 1e,f). Also, we previously investigated **A-pPrOzi-A**/CUR formulations by solution and solid state NMR[62] and found clear evidence for drug-polymer interactions in the hydrophilic pMeOx block. The lack of interaction of ATV with the pMeOx may therefore be responsible for the limited *LC* compared to CUR[66] or PTX[54] nanoformulations which exhibit *LC* of ≥ 50 wt.%. For reference, interactions between encapsulated ATV and the hydrophobic part of the polymeric drug carrier were observed previously for PLA-PEG-PLA-loaded ATV by FT-IR analysis.[39] Although stability of the aqueous **A-pBuOzi-A**/ATV formulations up to ATV feeds of 8 g/L was reasonably good, a minor loss in ATV content occurred in all formulations within 30 d storage (Figure 1d).

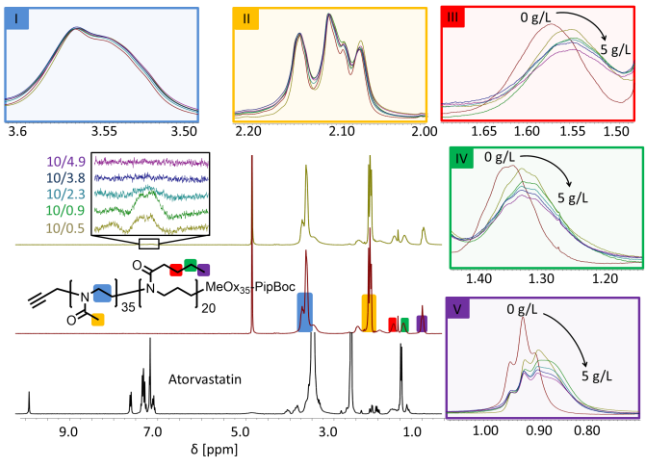

Figure 2: ^{1}H-NMR spectra (300 MHz, 298 K) of ATV (bottom black spectrum; DMSO-d_6), neat **A-pBuOzi-A** (middle red spectrum; D_2O) as well as **A-pBuOzi-A**/ATV = 10/0.5 g/L (top golden spectrum; D_2O). Inset shows enlarged region corresponding to aromatic ATV signals (700-fold increased signal intensity) with increasing ATV-loading (bottom to top; labelling is referred to **A-pBuOzi-A**/ATV = 10/y g/L). Enlarged sections of the signals corresponding to the hydrophilic shell of **A-pBuOzi-A** (I & II) as well as the hydrophobic core (III – V) in dependence of the ATV-loading. Intensities of spectra I-V were normalized to the methyl sidechain (II) of the hydrophilic shell. All formulations were prepared in H_2O, freeze-dried and subsequently redissolved in D_2O at ρ(polymer) = 10 g/L.

Shelf-life of drug-loaded micelles can potentially be increased by freeze-drying the aqueous formulations and redispersing them right before usage. POx and POzi based formulations of PTX[54] or CUR[66] have already displayed excellent redispersibility without the need of cryoprotectants. Similar, freeze-dried **A-pBuOzi-A**/ATV = 10/2 g/L formulations could be conveniently redispersed in H_2O (Figure 3 blue), PBS (red) or PBS containing 40 g/L bovine serum albumin (BSA, green) after 7 d storage of the freeze-dried formulations at ambient conditions. Redispersion in PBS containing 40 g/L BSA corresponding to the albumin concentration in blood was performed as preliminary test for upcoming *in vitro* and potential *in vivo* studies, as initially stable formulations can precipitate in the presence of proteins. The excellent stability in the presence of serum protein suggests that this formulation may be safely injected *i.v.*. When subjected to sink conditions, the ATV was readily released from the polymer micelles. After approx. about 18 h, ATV release was found to be quantitative (Figure S7).

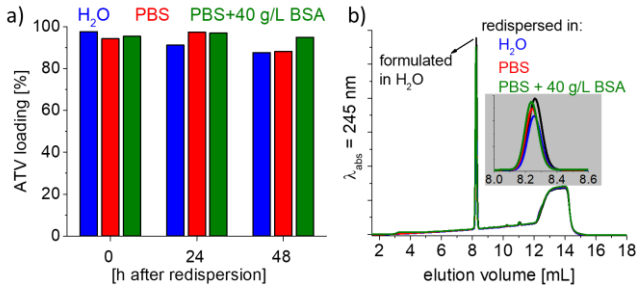

Figure 3: Residual aqueous ATV concentrations after redispersion of freeze-dried **A-pBuOzi-A**/ATV = 10/2 (g/L) formulations in H_2O (blue), PBS (red) or PBS containing 40 g/L bovine serum albumin (green). Loading [%] is referred to initial ATV concentration before freeze-drying. Prior to redispersion, the freeze-dried samples were stored for 7 d at ambient conditions (T ≈ 25 °C) under the exclusion of light; b) corresponding HPLC elugrams at λ_{abs} = 245 nm.

2D *in vitro* studies

Cytotoxicity of **A-pBuOzi-A**/ATV or ATV dissolved in DMSO against mouse glioma cells GL261 and CT-2A or human glioblastoma cells U87, U251 and U373 was evaluated after 24 h, 48 h and 72 h incubation (Figure 4). To the best of our knowledge, a potential growth inhibition or cytotoxicity of ATV against GL261, CT-2A and U373 has not previously been investigated. Except for CT-2A, cytotoxicity after 24 h incubation was moderate with half maximal inhibitory concentrations (IC_{50}) of 97 µM and higher. A similar low cytotoxicity of ATV after 24 h incubation (no decrease in proliferation up to [ATV] = 50 µM) compared to 48 h and 72 h was observed for human leukemic natural killer cells YT-INDY.[67] Furthermore, absence of cytotoxicity against U87 after 24 h incubation at [ATV] ≤ 100 µM was also observed by Yongjun *et al.*[23] In contrast, ATV exhibits a pronounced dose-dependent cytotoxicity after 48 h and 72 h incubation. The IC_{50} values for **A-pBuOzi-A**/ATV and DMSO/ATV were quite comparable (U87 (72 h); U373 (48 and 72 h)) and without significant differences. Generally, cytotoxicity increased from 48 h to 72 h incubation. Only for CT-2A, an unexpected increase in cell viability with IC_{50} values increasing from 33 µM (48 h) to 98 µM (72 h) occurred for DMSO/ATV. Furthermore, biphasic dose-response curves occurred in selected cases for DMSO/ATV (GL261) as well as **A-pBuOzi-A**/ATV (U251). Such multiphasic features are well known in cancer pharmacology[68] due to the presence of combined agonist (stimulatory or hormetic[69]) and antagonist effects as well as purely inhibitory features. Nevertheless, that with the same drug (ATV) both, sigmoidal and biphasic dose-responses occurred for a certain cell-line depending on the kind of formulation (DMSO or **A-pBuOzi-A**) is somehow surprising and needs to be evaluated further. Important to note, IC_{50} of DMSO/ATV for U87 (≈ 8 µM (48 h)[70] or ≈ 1.6 µM (48 h)[71]) or U251 (≈ 10 µM; 48 h[70]) cells reported in the literature were somewhat lower than the presently reported ones. However, different experimental setups (# cell passage, number of cells seeded, utilized assays) might have unintentionally caused such minor deviations. Important to note, inhibitory effects of ATV on growth and survival of U251 glioblastoma cells were attributed to decreased active Ras levels due to prenylation inhibition by ATV.[70] In the same study, 5 µM ATV inhibited proliferation of four different glioblastoma cell lines slightly stronger than temozolomide at 10 µM. In combination with the presented cytotoxicity of ATV on various glioblastoma cell lines this strongly supports the rationale to use ATV for glioblastoma chemotherapy. The dismal prognosis of glioblastomas is not only attributed to rapid tumor growth (and poor responses to chemo- and radiotherapy), but also to the diffuse intracerebral spread of migrating tumor cells.[72-73] We therefore examined the effects of ATV on the viability and cell migration of GBM6840 cells. This human cell line has been derived from a highly aggressive pediatric cerebellar glioblastoma multiforme[74], and is characterized by rapid cell proliferation and –migration *in vitro* and *in vivo*[75]. The GBM6840 cells were highly sensitive to ATV with an IC_{50} value of ~8 µM after 48 h treatment, irrespective of whether ATV was dissolved in DMSO or formulated with **A-pBuOzi-A** (Figure 5a; for representative examples of the original FACS results, the reader is referred to Figure S9). Importantly, neat **A-pBuOzi-A** did not cause cytotoxicity (viability > 80 %) up to high polymer concentrations of 10 g/L (Figure S9; for comparison: [**A-pBuOzi-A**] = 50 mg/L @ IC_{50}(**A-pBuOzi-A**/ATV), Figure 5a). We did not observe an effect of low ATV concentrations (2.5 or 5 µM) on the transwell-migration of GBM6840 cells towards epidermal growth factor (a prototypical chemoattractant for glioblastoma cells) even after 73 h of ATV treatment (Figure 5b). Important to note, these ATV concentrations were chosen because they did not

cause a substantial loss of cell viability (Figure S10), which would interfere with the cell migration assay. Thus, ATV appears to primarily affect GBM6840 cell viability, but not mobility at sub-toxic doses.

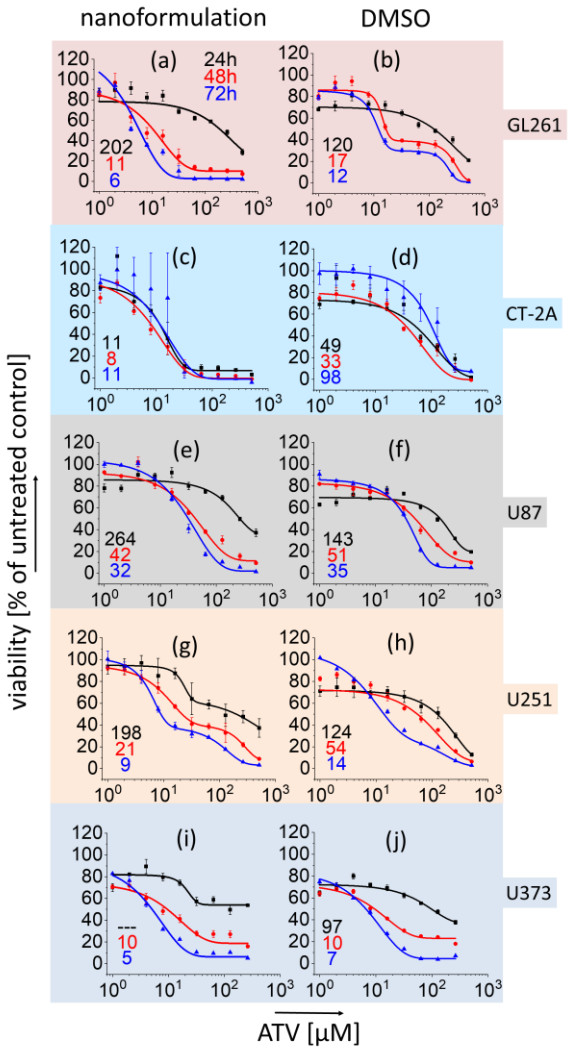

Figure 4: Concentration-dependent cell viability of **A-pBuOzi-A**/ATV (left column) or DMSO/ATV (right column) against mouse glioma cells GL261 (a,b) and CT-2A (c,d), or human glioblastoma cells U87 (e,f), U251 (g,h) and U373 (i,j). DMSO/ATV was prepared by dissolving 10 g/L (18 mM) ATV in DMSO upon dilution with PBS(-) to 1 g/L (1.8 mM) ATV and further dilution with cell specific medium to desired ATV concentrations. ATV-loaded **A-pBuOzi-A** micelles were prepared by thin-film method (ρ(**A-pBuOzi-A**/ATV) = 10/1 [g/L]) and diluted with cell-specific medium to desired ATV concentrations. Cell viability was determined (CCK-8 assay) after 24 h (black), 48 h (red) and 72 h (blue) ATV treatment. IC_{50} was determined per Boltzmann or biphasic dose-response fit using OriginPro 2019® and values for 24 h (black), 48 h (red) and 72 h (blue) are given in [µM] ATV in bottom left corner of each graph. Data are presented as mean ± SD (n = 3 (individual 96 well-plates) x 4 (wells per 96 plate)). Vehicles were used as control.

Spheroid cell cultures

So far, we could show that ATV was able to efficiently decrease cell-viability of various glioblastoma cell-lines in conventional 2D cell culture. However, cancer cells grown in 3D cell-clusters such as spheroids can behave significantly different from their monolayer counterparts[76] Also, accessibility of therapeutic agents and nanoparticles can be affected by the extracellular matrix *in vitro* in 3D cell culture and *in vivo*[77-81] In addition, we have also recently reported differences in tumor spheroids depending whether the API was administered in polymer micelles of the same type as discussed here or added as a ethanolic solution.[60] The multicellular structures resemble actual tissues better in terms of structural and functional properties and often exhibit an enhanced resistance against therapeutic compounds.[82] CT-2A cells were chosen due to their ability to form spheroids without the need of specialized devices or additives. Furthermore, the difference in cytotoxicity between **A-pBuOzi-A** (Figure 4c) and DMSO (Figure 4d) formulated ATV was most pronounced in this cell line. Spheroids were obtained by simply seeding the cells (5 x 10^3 cells/well) in U-bottom shaped 96 well-plates. Similar to conventional 2D-cell culture, both ATV formulations strongly decreased CT-2A cell viability in a concentration-dependent manner (Figure 6a,b). Here, **A-pBuOzi-A**/ATV again was clearly more effective than DMSO/ATV. Similar to conventional 2D cell culture (Figure 4d), cell viability in the spheroid model increased from 48 h (50 %) to 72 h (55 %) treatment with 8 µM DMSO/ATV. Unexpectedly, cytotoxicity of **A-pBuOzi-A**/ATV was higher in the spheroid model (Figure 6a,b) than in conventional 2D cell-culture (Figure 4c). A similarly high activity of ATV in 3D cell-culture was also observed for U87 glioma spheroids incorporated into a fibrin gel with IC_{50} (48 h) ≈ 10 µM.[76] Besides induction of apoptosis, migration and invasion of the U87 cells were inhibited in a dose-dependent manner in this case.

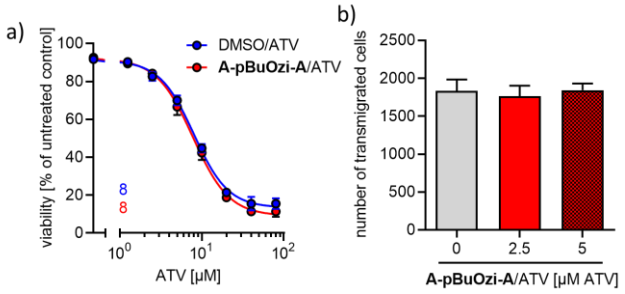

Figure 5: a) Concentration-dependent effect of **A-pBuOzi-A**/ATV (red) or DMSO/ATV (blue) on GBM6840 human glioblastoma cell viability after 48 h treatment. ATV was formulated or solubilized as described in the legend of Fig. 4. IC_{50} values were determined by non-linear regression (log(inhibitor) vs. response – variable slope (four parameters)) using GraphPad Prism v7.04. Data are means ± SEM of *n*=3 independent experiments. b) Effect of **A-pBuOzi-A**/ATV on the epidermal growth factor-induced migration of GBM6840 cells through transwells. In total, eight (control and 2.5 µM ATV) or four (5 µM ATV) transwells were analyzed. Data are means ± SEM of *n*=2 independent experiments.

To further challenge ATV as potential chemotherapeutic agent against glioblastoma, its activity against spheroids composed of mouse-derived, glioblastoma cancer-stem cells (CSCs) was evaluated (Figure 6c,d). CSCs are cancer cells found within tumors with the ability of self-renewal, generation of daughter cells of various phenotypes and differentiation into phenotypically diverse populations of cells.[83] Therefore, small populations of CSCs present after treatment can cause rapid cancer relapse as well as metastasis. Unfortunately this is favored by an increased resistance of CSCs to various otherwise unfavorable conditions[84] including increased resistance against radiotherapy[85] and chemotherapy[86]. To the best of our knowledge, the cytotoxicity of ATV against glioblastoma stem cells or cancer stem cells in general has not been investigated before. However, for another statin, pitavastatin, autophagy induction in patient-derived stem cell-like primary GBM (as well as delayed U87 GBM tumor growth *in vivo*) was observed.[21] Similar

to CT-2A, the bRiTS-G2 brain tumor initiating cells rapidly formed spheroids when placed in U-bottom shaped 96 wells. Surprisingly, **A-pBuOzi-A**/ATV and to a lesser extent DMSO/ATV were highly active against the tumor spheres after 48 h and 72 h incubation (Figure 6c,d). Interestingly, a recently reported micellar mitotane nanoformulation of **A-pBuOx-A** was also slightly more active than mitotane simply dissolved in EtOH against adrenocortical NCI-H295R cells in a 3D tumor spheroid model ($IC_{50,48h}$ = 43 µM & 47 µM for nanoformulated & EtOH-dissolved mitotane, respectively).[60] It has been reported that the extracellular matrix present in 3D cell culture and *in vivo* can have a profound effect on drug penetration and therefore efficacy[77-81]. At this point, we can only hypothesize that that ATV nanoformulation may also be able to penetrate the spheroids better and this, result in a more pronounced growth inhibition. Important to note, the pronounced cytotoxicity of **A-pBuOzi-A**/ATV after 72 h treatment determined by CellTiterGlo®-3D luminescence assay was confirmed when quantifying the cell-viability by the intrinsic fluorescence of the GFP expressing bRiTS-G2 cells (inset Figure 6d). Although the absolute values slightly differed, both measurement techniques gave comparable results.

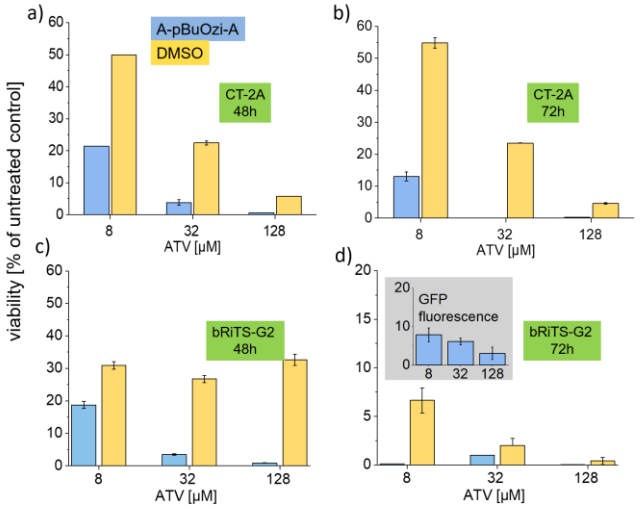

Figure 6: Concentration-dependent cytotoxicity of **A-pBuOzi-A**/ATV (blue) or DMSO/ATV (yellow) against spheroids of mouse glioma cells CT-2A after a) 48 h or b) 72 h treatment or against spheroids of mouse brain tumor initiating bRiTS-G2 cells after c) 48 h or d) 72 h treatment. DMSO/ATV was prepared by dissolving 10 g/L ATV in DMSO upon dilution with PBS(-) to 1 g/L ATV and further dilution with cell specific medium to desired ATV concentrations. ATV-loaded **A-pBuOzi-A** micelles were prepared by thin-film method (ρ(**A-pBuOzi-A**/ATV) = 10/1 [g/L]) and diluted with cell-specific medium to desired ATV concentrations. Spheroids were obtained by seeding the cells in U-bottom shaped 96 well-plates at 5 x 10^3 cells/well. Cell viability was determined by CellTiter-Glo® 3D assay. Data are presented as mean ± SD (n = 3 (individual 96 well-plates) x 4 (wells per 96 plate)). As a control, cell viability of bRiTS-G2 spheroids treated with **A-pBuOzi-A** formulated ATV was determined by intrinsic fluorescence of GFP-expressing bRiTS-G2 cells (inset Figure d). Date are presented as mean ± SD (n = 2 (individual 96 well-plates) x 4 (wells per 96 plate)).

ATV permeability through artificial blood-brain barrier

The pronounced cytotoxicity of ATV against glioblastoma in 2D cell culture (Figure 4, 5) as well as 3D spheroid models (Figure 6) suggests its potential for GBM chemotherapy. However, in order to unfold its therapeutic potential *in vivo*, ATV needs to reach tumor site first. This includes permeation through the BBB after e.g. parenteral administration.[87] Several sophisticated *in vitro* BBB models were developed in recent years to resemble the situation *in vivo*.[88-90] Apart from the cellular barrier, the *in vivo* the situation is also complicated by flow, which has been taken into consideration by some recent models.[91] One promising approach are models based on human induced pluripotent stem cells (hiPSCs) derived BBB endothelial cells.[55, 92] Using such a hiPSC-derived model, physiological characteristics like high transendothelial electrical resistances (TEER) up to 2,500 Ω·cm², distinct upregulation of typical BBB genes as well as the formation of an *in vivo*-like tight junction (TJ) network could be achieved.[55] The hiPSC-derived BBB endothelial cells were seeded on top of a transwell insert and subsequently the permeability of ATV from the apical to the basolateral compartment was investigated (Figure 7a). A ratio of **A-pBuOzi-A**/ATV = 10/1 g/L was chosen due to the small size of the respective ATV-loaded micelles (Figure 1e,f) potentially facilitating transcellular permeability, assuming integrity of the drug loaded micelles. The latter is not necessarily given due to e.g. potential transfer of incorporated ATV to proteins[93] present in solution as observed for **A-pBuOx-A**/PTX *in vitro* and *in vivo*[94]. ATV was either solubilized with **A-pBuOzi-A** or dissolved in DMSO and applied at 90 µM (50 mg/L) as well as 150 µM (83 mg/L). For comparison, oral administration of 40 mg ATV in hypercholesterolaemic haemodialysis patients resulted in ATV peak plasma concentrations of 28.6 ± 15.2 µg/L (51 nM; reached 1-2 hours after initial administration), together with the active metabolites o- and p-OH ATV (8.1 and 0.6 µg/L) as well as inactive 3-lactone metabolites (44.2 µg/L).[95] This strongly suggests that the necessary ATV plasma concentrations to achieve growth inhibition *in vivo* will likely not be achievable via the oral route and a formulation suitable for parenteral application is needed. At both concentrations, no pronounced cytotoxic effects of ATV on the endothelial cells of the artificial BBB were observed after 4 h incubation, ensuring the integrity of the monolayer during the course of the experiment (Figure S11a). After 24 h incubation, again no cytotoxicity up to ATV = 90 µM occurred (Figure S11b). Only at ATV = 150 µM, cell viability decreased to 41 % and 49 % for DMSO/ATV and **A-pBuOzi-A**/ATV, respectively. ATV was quantified in the apical and basolateral chamber after 4 h and 24 h incubation. To ensure the permeability analysis of **A-pBuOzi-A**/ATV and DMSO/ATV through the BBB endothelial cell layer itself, transwells without cells were always included to correct the permeation values for the barrier formed by the membrane support. In all cases, a higher ATV concentration occurred on the basolateral side of the latter compared to wells containing cells (Figure S12). Furthermore, diffusion through the blank membrane was more or less the same for **A-pBuOzi-A**/ATV and DMSO/ATV therefore excluding variances due to different diffusion profiles. With respect to the wells without cells, the ATV transport through the BBB was less efficient at apical ATV feed of 150 µM, compared to 90 µM (Figure 7b). Nevertheless, absolute basolateral ATV concentrations increased from 4 h to 24 h incubation and from $[ATV_{feed}]$ = 90 µM to 150 µM in all samples (Figure S12). For both ATV concentrations and time-points, ATV permeability was slightly higher for **A-pBuOzi-A**/ATV than for DMSO/ATV, however, the differences were within the standard deviations (Figure 7b). This suggests that our nanoformulation does not alter the permeation profile of ATV through this BBB *in vitro* model significantly. Whether this is due to a rapid release of ATV from the micelles to e.g. proteins present in medium or e.g. the disintegration of the ATV-loaded micelles at the cell-membrane – not further improving endocytosis or transcellular delivery – remains to be elucidated. However, rapid disintegration of drug-loaded micelles within the blood stream is not necessarily detrimental regarding therapeutic efficacy, as evidenced by POx/PTX nanoformulations,

which exhibit an excellent therapeutic efficacy *in vivo*.[94] Interestingly, the proportional basolateral ATV concentration with respect to the wells without cells increased from 4 h to 24 h incubation for both, DMSO/ATV and **A-pBuOzi-A**/ATV (Figure 7b). Taking a closer look at the TEER values showed a decrease in resistance after 24 h at both ATV feed concentrations of 90 and 150 µM (Figure 7c,d). Even though we observed no ATV cytotoxicity up to 90 µM (Figure S11), the integrity of the BBB is apparently affected, probably through a loosening of the tight junctions. This may be an early indication of cytotoxic effects. Although the transport across the BBB is not significantly improved, the presented novel POzi/ATV formulation may allow much higher ATV serum concentrations, compared to oral administration or alternative drug delivery systems, as much higher ATV concentrations can potentially be administered. Therefore, therapeutic doses may be reached, even without improved transport across the BBB.

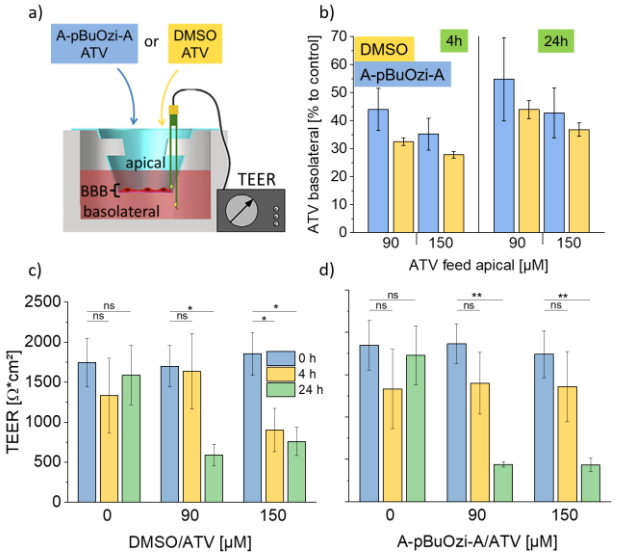

Figure 7: a) Setup to investigate the permeability of ATV through hiPSC-derived *in vitro* models of the human blood-brain barrier (BBB) in a transwell setup (image adapted from Appelt-Menzel *et al.*[55]); b) **A-pBuOzi-A**/ATV = 10/1 [g/L] (blue) or DMSO/ATV (yellow) were diluted with cell specific medium to desired ATV concentrations of 90 µM or 150 µM and applied to the apical side of the transwells. Subsequently, basolateral ATV concentrations were quantified after 4 h and 24 h incubation with respect to the permeability through wells without cells (= control). Permeation was determined in three individual transwell-plates each containing the respective samples in duplicates. Data are presented as mean ± SD; n = 3; TEER values of non-treated BBB as well as treatment with c) DMSO/ATV or d) **A-pBuOzi-A**/ATV for either 0 h (before treatment, blue bars), 4 h (yellow bars) or 24 h (green bars) TEER values were determined in three positions of three individual transwell-plates each containing the respective samples in duplicates. Data are presented as mean ± SEM (n = 3, *p<0.05, **p<0.01).

Furthermore, co-administration with agents temporarily permealizing the BBB could help to increase the ATV concentration across the BBB. Such agent could be SP1049C or small molecules known to permealize the BBB. Possibly, such agent could be coformulated with ATV and therefore improve co-delivery of both APIs.

CONCLUSION

We presented a novel nanoformulation of atorvastatin (ATV), a statin with potential in the treatment of various tumors, including glioblastoma. A moderate increase in the apparent aqueous solubility of ATV by a factor of 100 was achieved, but the sizes of the formed particles are too large for intravenous administration at the highest drug loading. Only at low drug loading < 10 wt.%, nanoformulations (D_h < 50 nm) were obtained while at higher loading, large submicron particles were formed. The encapsulated ATV was fully bioactive and exhibited IC_{50} values in the low to medium micromolar range in a panel of different glioblastoma cell lines with no systematic difference between free, DMSO solubilized ATV and ATV solubilized using polymer micelles. In contrast, in tumor spheroids prepared from CT-2A mouse glioma and bRiTS-G2 mouse glioma cancer stem cells, the micellar formulation was consistently more active. Very interestingly, we found particularly high activity against bRiTS-G2 with minimal cell survival even at low micromolar ATV concentrations. Finally, transport through a blood-brain-barrier *in vitro* model based on differentiated human induced pluripotent stem cells was tested and revealed no significant difference for the transport of micellar ATV and ATV dissolved by DMSO. However, as our novel micellar ATV formulations may enable much higher serum concentration of ATV, therapeutic doses may still be possible. However, this must be carefully investigated in more relevant *in vitro* models, possibly including perfusion or careful *in vivo* studies. Especially by combination with other active agents, micellar ATV may have potential for the treatment of glioblastoma, but future studies must carefully assess safety of micellar ATV at elevated concentrations.

ACKNOWLEDGEMENT

This work was supported by the Free State of Bavaria and the Deutsche Forschungsgemeinschaft (Project number 398461692, awarded to R.L.). Moreover, M.M.L. would like to thank the Evonik Foundation for providing a doctoral fellowship. We thank Christian May for technical support. Furthermore, we thank Dr. Jorge Tapia-Perez for inspiring this study.

SUPPORTING INFORMATION

HPLC drug quantification, images of tumor spheroids, nanoformulation stability, ^{1}H-NMR spectra of polymer A-pBuOzi-A and ATV, changes in NMR signal intensity with drug loading, in vitro drug release, flow cytometry data of GBM6840 viability and GBM6840 morphology images, viability of hiPS-based BBB endothelial cells and ATV permeability through hiPS-based BBB.

REFERENCES

1. Delgado-López, P. D.; Corrales-García, E. M., Survival in glioblastoma: a review on the impact of treatment modalities. *Clin. Transl. Oncol.* **2016,** *18* (11), 1062-1071.
2. Ostrom, Q. T.; Gittleman, H.; Liao, P.; Rouse, C.; Chen, Y.; Dowling, J.; Wolinsky, Y.; Kruchko, C.; Barnholtz-Sloan, J., CBTRUS statistical report: primary brain and central nervous system tumors diagnosed in the United States in 2007-2011. *Neuro-Oncol.* **2014,** *16 Suppl 4* (Suppl 4), iv1-iv63.
3. Stupp, R.; Hegi, M. E.; Mason, W. P.; van den Bent, M. J.; Taphoorn, M. J. B.; Janzer, R. C.; Ludwin, S. K.; Allgeier, A.; Fisher, B.; Belanger, K.; Hau, P.; Brandes, A. A.; Gijtenbeek, J.; Marosi, C.; Vecht, C. J.; Mokhtari, K.; Wesseling, P.; Villa, S.; Eisenhauer, E.; Gorlia, T.; Weller, M.; Lacombe, D.; Cairncross, J. G.; Mirimanoff, R.-O., Effects of radiotherapy with concomitant and adjuvant temozolomide versus radiotherapy alone on survival in glioblastoma in a randomised phase III study: 5-year analysis of the EORTC-NCIC trial. *Lancet Oncol.* **2009,** *10* (5), 459-466.
4. Xie, Q.; Mittal, S.; Berens, M. E., Targeting adaptive glioblastoma: an overview of proliferation and invasion. *Neuro-Oncol.* **2014,** *16* (12), 1575-1584.

5. Osuka, S.; Van Meir, E. G., Overcoming therapeutic resistance in glioblastoma: the way forward. *J. Clin. Investig.* **2017,** *127* (2), 415-426.
6. Haar, C. P.; Hebbar, P.; Wallace, G. C.; Das, A.; Vandergrift, W. A.; Smith, J. A.; Giglio, P.; Patel, S. J.; Ray, S. K.; Banik, N. L., Drug Resistance in Glioblastoma: A Mini Review. *Neurochem. Res.* **2012,** *37* (6), 1192-1200.
7. Pardridge, W. M., Drug transport across the blood-brain barrier. *J. Cereb. Blood Flow Metab.* **2012,** *32* (11), 1959-1972.
8. Pandey, P. K.; Sharma, A. K.; Gupta, U., Blood brain barrier: An overview on strategies in drug delivery, realistic in vitro modeling and in vivo live tracking. *Tissue barriers* **2015,** *4* (1), e1129476-e1129476.
9. Lee, S. Y., Temozolomide resistance in glioblastoma multiforme. *Genes & diseases* **2016,** *3* (3), 198-210.
10. Farnier, M.; Davignon, J., Current and future treatment of hyperlipidemia: the role of statins. *Am. J. Cardiol.* **1998,** *82* (4), 3J-10J.
11. Liao, J. K., Effects of statins on 3-hydroxy-3-methylglutaryl coenzyme a reductase inhibition beyond low-density lipoprotein cholesterol. *Am. J. Cardiol.* **2005,** *96* (5A), 24F-33F.
12. Hindler, K.; Cleeland, C. S.; Rivera, E.; Collard, C. D., The Role of Statins in Cancer Therapy. *The Oncologist* **2006,** *11* (3), 306-315.
13. Shellman, Y. G.; Ribble, D.; Miller, L.; Gendall, J.; VanBuskirk, K.; Kelly, D.; Norris, D. A.; Dellavalle, R. P., Lovastatin-induced apoptosis in human melanoma cell lines. *Melanoma Res.* **2005,** *15* (2), 83-89.
14. Koyuturk, M.; Ersoz, M.; Altiok, N., Simvastatin induces proliferation inhibition and apoptosis in C6 glioma cells via c-jun N-terminal kinase. *Neurosci. Lett.* **2004,** *370* (2), 212-217.
15. Girgert, R.; Vogt, Y.; Becke, D.; Bruchelt, G.; Schweizer, P., Growth inhibition of neuroblastoma cells by lovastatin and l-ascorbic acid is based on different mechanisms. *Cancer Lett.* **1999,** *137* (2), 167-172.
16. Sassano, A.; Katsoulidis, E.; Antico, G.; Altman, J. K.; Redig, A. J.; Minucci, S.; Tallman, M. S.; Platanias, L. C., Suppressive Effects of Statins on Acute Promyelocytic Leukemia Cells. *Cancer Res.* **2007,** *67* (9), 4524.
17. Yanae, M.; Tsubaki, M.; Satou, T.; Itoh, T.; Imano, M.; Yamazoe, Y.; Nishida, S., Statin-induced apoptosis via the suppression of ERK1/2 and Akt activation by inhibition of the geranylgeranyl-pyrophosphate biosynthesis in glioblastoma. *J. Exp. Clin. Canc. Res.* **2011,** *30* (1), 74.
18. Pisanti, S.; Picardi, P.; Ciaglia, E.; D'Alessandro, A.; Bifulco, M., Novel prospects of statins as therapeutic agents in cancer. *Pharmacol. Res.* **2014,** *88*, 84-98.
19. Gizzo, S.; Quaranta, M.; Nardelli, G. B.; Noventa, M., Lipophilic Statins as Anticancer Agents: Molecular Targeted Actions and Proposal in Advanced Gynaecological Malignancies. *Curr. Drug Targets* **2015,** *16* (10), 1142-1159.
20. Prasanna, P.; Thibault, A.; Liu, L.; Samid, D., Lipid Metabolism as a Target for Brain Cancer Therapy: Synergistic Activity of Lovastatin and Sodium Phenylacetate Against Human Glioma Cells. *J. Neurochem.* **1996,** *66* (2), 710-716.
21. Jiang, P.; Mukthavaram, R.; Chao, Y.; Nomura, N.; Bharati, I. S.; Fogal, V.; Pastorino, S.; Teng, D.; Cong, X.; Pingle, S. C.; Kapoor, S.; Shetty, K.; Aggrawal, A.; Vali, S.; Abbasi, T.; Chien, S.; Kesari, S., In vitro and in vivo anticancer effects of mevalonate pathway modulation on human cancer cells. *Br. J. Cancer* **2014,** *111*, 1562.
22. Bayat, N.; Ebrahimi-Barough, S.; Norouzi-Javidan, A.; Saberi, H.; Tajerian, R.; Ardakan, M. M. M.; Shirian, S.; Ai, A.; Ai, J., Apoptotic effect of atorvastatin in glioblastoma spheroids tumor cultured in fibrin gel. *Biomed. Pharmacother.* **2016,** *84*, 1959-1966.
23. Yongjun, Y.; Shuyun, H.; Lei, C.; Xiangrong, C.; Zhilin, Y.; Yiquan, K., Atorvastatin suppresses glioma invasion and migration by reducing microglial MT1-MMP expression. *J. Neuroimmunol.* **2013,** *260* (1), 1-8.
24. Bayat, N.; Ebrahimi-Barough, S.; Norouzi-Javidan, A.; Saberi, H.; Ardakan, M. M. M.; Ai, A.; Soleimannejad, M.; Ai, J., Anti-inflammatory Effects of Atorvastatin by Suppressing TRAF3IP2 and IL-17RA in Human Glioblastoma Spheroids Cultured in a Three-dimensional Model: Possible Relevance to Glioblastoma Treatment. *Mol. Neurobiol.* **2018,** *55* (3), 2102-2110.
25. Colotta, F.; Allavena, P.; Sica, A.; Garlanda, C.; Mantovani, A., Cancer-related inflammation, the seventh hallmark of cancer: links to genetic instability. *Carcinogenesis* **2009,** *30* (7), 1073-1081.
26. Yeung, Y. T.; McDonald, K. L.; Grewal, T.; Munoz, L., Interleukins in glioblastoma pathophysiology: implications for therapy. *Br. J. Pharmacol.* **2013,** *168* (3), 591-606.
27. Shimada, K.; Skouta, R.; Kaplan, A.; Yang, W. S.; Hayano, M.; Dixon, S. J.; Brown, L. M.; Valenzuela, C. A.; Wolpaw, A. J.; Stockwell, B. R., Global survey of cell death mechanisms reveals metabolic regulation of ferroptosis. *Nat. Chem. Biol.* **2016,** *12*, 497.
28. Altwairgi, A. K.; Alghareeb, W.; Alnajjar, F.; Alsaeed, E.; Balbaid, A.; Alhussain, H.; Aldanan, S.; Orz, Y.; Lari, A.; Alsharm, A., Phase II study of atorvastatin in combination with radiotherapy and temozolomide In patients with glioblastoma (ART): interim analysis report. *Ann. Oncol.* **2016,** *27* (suppl_6).
29. Tang, T.-T.; Song, Y.; Ding, Y.-J.; Liao, Y.-H.; Yu, X.; Du, R.; Xiao, H.; Yuan, J.; Zhou, Z.-H.; Liao, M.-Y.; Yao, R.; Jevallee, H.; Shi, G.-P.; Cheng, X., Atorvastatin upregulates regulatory T cells and reduces clinical disease activity in patients with rheumatoid arthritis. *J. Lipid Res.* **2011,** *52* (5), 1023-1032.
30. Banks, W. A., Characteristics of compounds that cross the blood-brain barrier. *BMC Neurol.* **2009,** *9 Suppl 1* (Suppl 1), S3-S3.
31. David, J. B., ABC Transporters and the Blood-Brain Barrier. *Curr. Pharm. Des.* **2004,** *10* (12), 1295-1312.
32. Tamai, I.; Tsuji, A., Transporter-Mediated Permeation of Drugs Across the Blood–Brain Barrier. *J. Pharm. Sci.* **2000,** *89* (11), 1371-1388.
33. Tsuji, A.; Saheki, A.; Tamai, I.; Terasaki, T., Transport mechanism of 3-hydroxy-3-methylglutaryl coenzyme A reductase inhibitors at the blood-brain barrier. *J. Pharmacol. Exp. Ther.* **1993,** *267* (3), 1085.
34. Saheki, A.; Terasaki, T.; Tamai, I.; Tsuji, A., In Vivo and in Vitro Blood–Brain Barrier Transport of 3-Hydroxy-3-Methylglutaryl Coenzyme A (HMG-CoA) Reductase Inhibitors. *Pharm. Res.* **1994,** *11* (2), 305-311.
35. Schultz, B. G.; Patten, D. K.; Berlau, D. J., The role of statins in both cognitive impairment and protection against dementia: a tale of two mechanisms. *Transl. Neurodegener.* **2018,** *7*, 5-5.
36. Sahebzamani, F. M.; Munro, C. L.; Marroquin, O. C.; Diamond, D. M.; Keller, E.; Kip, K. E., Examination of the FDA Warning for Statins and Cognitive Dysfunction. *J. Pharmacovigil.* **2014,** *2* (4), 1000141-100015.

37. Shi, J.; Kantoff, P. W.; Wooster, R.; Farokhzad, O. C., Cancer nanomedicine: progress, challenges and opportunities. *Nat. Rev. Cancer* **2017,** *17*, 20-37.
38. Cabral, H.; Miyata, K.; Osada, K.; Kataoka, K., Block Copolymer Micelles in Nanomedicine Applications. *Chem. Rev.* **2018,** *118* (14), 6844-6892.
39. Danafar, H.; Rostamizadeh, K.; Hamidi, M., Polylactide/poly(ethylene glycol)/polylactide triblock copolymer micelles as carrier for delivery of hydrophilic and hydrophobic drugs: a comparison study. *J. Pharm. Investig.* **2017,** *48*, 381-391.
40. Andalib, S.; Molhemazar, P.; Danafar, H., In vitro and in vivo delivery of atorvastatin: A comparative study of anti-inflammatory activity of atorvastatin loaded copolymeric micelles. *J. Biomatr. Appl.* **2017,** *32* (8), 1127-1138.
41. Xu, P.; Yu, H.; Zhang, Z.; Meng, Q.; Sun, H.; Chen, X.; Yin, Q.; Li, Y., Hydrogen-bonded and reduction-responsive micelles loading atorvastatin for therapy of breast cancer metastasis. *Biomaterials* **2014,** *35* (26), 7574-7587.
42. Mekhail, G. M.; Kamel, A. O.; Awad, G. A. S.; Mortada, N. D., Anticancer effect of atorvastatin nanostructured polymeric micelles based on stearyl-grafted chitosan. *Int. J. Biol. Macromol.* **2012,** *51* (4), 351-363.
43. S, S.; C. H, A.; C, G. P. D.; B, R.; Ravindran, A., BSA Nanoparticle Loaded Atorvastatin Calcium - A New Facet for an Old Drug. *PLoS One* **2014,** *9* (2), e86317.
44. Şimşek, S.; Eroğlu, H.; Kurum, B.; Ulubayram, K., Brain targeting of Atorvastatin loaded amphiphilic PLGA-b-PEG nanoparticles. *J. Microencapsul.* **2013,** *30* (1), 10-20.
45. Batrakova, E. V.; Li, S.; Miller, D. W.; Kabanov, A. V., Pluronic P85 Increases Permeability of a Broad Spectrum of Drugs in Polarized BBMEC and Caco-2 Cell Monolayers. *Pharm. Res.* **1999,** *16* (9), 1366-1372.
46. Price, T. O.; Farr, S. A.; Yi, X.; Vinogradov, S.; Batrakova, E. V.; Banks, W. A.; Kabanov, A. V., Transport Across the Blood-Brain Barrier of Pluronic Leptin. *J. Pharmacol. Exp. Ther.* **2010**, jpet.109.158147.
47. Tong, J.; Yi, X.; Luxenhofer, R.; Banks, W. A.; Jordan, R.; Zimmerman, M. C.; Kabanov, A. V., Conjugates of Superoxide Dismutase 1 with Amphiphilic Poly(2-oxazoline) Block Copolymers for Enhanced Brain Delivery: Synthesis, Characterization and Evaluation in Vitro and in Vivo. *Mol. Pharm.* **2013,** *10* (1), 360-377.
48. Banks, W. A.; Gertler, A.; Solomon, G.; Niv-Spector, L.; Shpilman, M.; Yi, X.; Batrakova, E.; Vinogradov, S.; Kabanov, A. V., Principles of strategic drug delivery to the brain (SDDB): Development of anorectic and orexigenic analogs of leptin. *Physiol. Behav.* **2011,** *105* (1), 145-149.
49. Hemmelmann, M.; Knoth, C.; Schmitt, U.; Allmeroth, M.; Moderegger, D.; Barz, M.; Koynov, K.; Hiemke, C.; Rosch, F.; Zentel, R., HPMA based amphiphilic copolymers mediate central nervous effects of domperidone. *Macromol Rapid Commun* **2011,** *32* (9-10), 712-7.
50. Hemmelmann, M.; Metz, V. V.; Koynov, K.; Blank, K.; Postina, R.; Zentel, R., Amphiphilic HPMA-LMA copolymers increase the transport of Rhodamine 123 across a BBB model without harming its barrier integrity. *J Control Release* **2012,** *163* (2), 170-7.
51. Clemens-Hemmelmann, M.; Kuffner, C.; Metz, V.; Kircher, L.; Schmitt, U.; Hiemke, C.; Postina, R.; Zentel, R., Amphiphilic Copolymers Shuttle Drugs Across the Blood-Brain Barrier. *Macromol Biosci* **2016,** *16* (5), 655-65.
52. Witte, H.; Seeliger, W., Cyclische Imidsäureester aus Nitrilen und Aminoalkoholen. *Liebigs Ann. Chem.* **1974,** *1974* (6), 996-1009.
53. Lübtow, M. M.; Haider, M. S.; Kirsch, M.; Klisch, S.; Luxenhofer, R., Like Dissolves Like? A Comprehensive Evaluation of Partial Solubility Parameters to Predict Polymer–Drug Compatibility in Ultrahigh Drug-Loaded Polymer Micelles. *Biomacromolecules* **2019,** *20* (8), 3041-3056.
54. Luxenhofer, R.; Schulz, A.; Roques, C.; Li, S.; Bronich, T. K.; Batrakova, E. V.; Jordan, R.; Kabanov, A. V., Doubly amphiphilic poly(2-oxazoline)s as high-capacity delivery systems for hydrophobic drugs. *Biomaterials* **2010,** *31* (18), 4972-4979.
55. Appelt-Menzel, A.; Cubukova, A.; Günther, K.; Edenhofer, F.; Piontek, J.; Krause, G.; Stüber, T.; Walles, H.; Neuhaus, W.; Metzger, M., Establishment of a Human Blood-Brain Barrier Co-culture Model Mimicking the Neurovascular Unit Using Induced Pluri- and Multipotent Stem Cells. *Stem Cell Rep.* **2017,** *8* (4), 894-906.
56. Lübtow, M. M.; Hahn, L.; Haider, M. S.; Luxenhofer, R., Drug Specificity, Synergy and Antagonism in Ultrahigh Capacity Poly(2-oxazoline)/Poly(2-oxazine) based Formulations. *J. Am. Chem. Soc.* **2017,** *139* (32), 10980-10983.
57. Hahn, L.; Lübtow, M. M.; Lorson, T.; Schmitt, F.; Appelt-Menzel, A.; Schobert, R.; Luxenhofer, R., Investigating the Influence of Aromatic Moieties on the Formulation of Hydrophobic Natural Products and Drugs in Poly(2-oxazoline)-Based Amphiphiles. *Biomacromolecules* **2018,** *19* (7), 3119-3128.
58. Lübtow, M. M.; Keßler, L.; Appelt-Menzel, A.; Lorson, T.; Gangloff, N.; Kirsch, M.; Dahms, S.; Luxenhofer, R., More Is Sometimes Less: Curcumin and Paclitaxel Formulations Using Poly(2-oxazoline) and Poly(2-oxazine)-Based Amphiphiles Bearing Linear and Branched C9 Side Chains. *Macromol. Biosci.* **2018,** *18* (11), 1800155.
59. Seo, Y.; Schulz, A.; Han, Y.; He, Z.; Bludau, H.; Wan, X.; Tong, J.; Bronich, T. K.; Sokolsky, M.; Luxenhofer, R.; Jordan, R.; Kabanov, A. V., Poly(2-oxazoline) block copolymer based formulations of taxanes: effect of copolymer and drug structure, concentration, and environmental factors. *Polym. Adv. Technol.* **2015,** *26* (7), 837-850.
60. Haider, M. S.; Schreiner, J.; Kendl, S.; Kroiß, M.; Luxenhofer, R., A Micellar Mitotane Formulation with High Drug-Loading and Solubility: Physico-Chemical Characterization and Cytotoxicity Studies in 2D and 3D in Vitro Tumor Models. *Macromol. Biosci.* **2019**, doi: 10.1002/mabi.201900178.
61. Lübtow, M. M.; Marciniak, H.; Schmiedel, A.; Roos, M.; Lambert, C.; Luxenhofer, R., Ultra-high to ultra-low drug loaded micelles: Probing host-guest interactions by fluorescence spectroscopy. *Chem.: Eur. J.* **2019,** *25*, 12601-12610.
62. Pöppler, A.-C.; Lübtow, M. M.; Schlauersbach, J.; Wiest, J.; Meinel, L.; Luxenhofer, R., Loading dependent Structural Model of Polymeric Micelles Encapsulating Curcumin by Solid-State NMR Spectroscopy. *Angew. Chem. Int. Ed.* **2019,** (ja), doi:10.1002/anie.201908914.
63. Danson, S.; Ferry, D.; Alakhov, V.; Margison, J.; Kerr, D.; Jowle, D.; Brampton, M.; Halbert, G.; Ranson, M., Phase I dose escalation and pharmacokinetic study of pluronic polymer-bound doxorubicin (SP1049C) in patients with advanced cancer. *Br. J. Cancer* **2004,** *90* (11), 2085-2091.
64. Kabanov, A. V.; Batrakova, E. V.; Miller, D. W., Pluronic® block copolymers as modulators of drug efflux transporter activity in the blood–brain barrier. *Adv. Drug Deliv. Rev.* **2003,** *55* (1), 151-164.
65. Kabanov, A. V.; Batrakova, E. V.; Alakhov, V. Y., Pluronic® block copolymers as novel polymer therapeutics for drug and gene delivery. *J. Control. Release* **2002,** *82* (2), 189-212.

66. Lübtow, M. M.; Nelke, L. C.; Seifert, J.; Kühnemundt, J.; Sahay, G.; Dandekar, G.; Nietzer, S. L.; Luxenhofer, R., Drug induced micellization into ultra-high capacity and stable curcumin nanoformulations: Physico-chemical characterization and evaluation in 2D and 3D in vitro models. *J. Control. Release* **2019,** *303*, 162-180.
67. Crosbie, J.; Magnussen, M.; Dornbier, R.; Iannone, A.; Steele, T. A., Statins inhibit proliferation and cytotoxicity of a human leukemic natural killer cell line. *Biomark. Res.* **2013,** *1* (1), 33-33.
68. Di Veroli, G. Y.; Fornari, C.; Goldlust, I.; Mills, G.; Koh, S. B.; Bramhall, J. L.; Richards, F. M.; Jodrell, D. I., An automated fitting procedure and software for dose-response curves with multiphasic features. *Sci. Rep.* **2015,** *5*, 14701.
69. Calabrese, E. J., Biphasic dose responses in biology, toxicology and medicine: Accounting for their generalizability and quantitative features. *Environ. Pollut.* **2013,** *182*, 452-460.
70. Peng, P.; Wei, W.; Long, C.; Li, J., Atorvastatin augments temozolomide's efficacy in glioblastoma via prenylation-dependent inhibition of Ras signaling. *Biochem. Biophys. Res. Commun.* **2017,** *489* (3), 293-298.
71. Tapia-Pérez, J. H.; Kirches, E.; Mawrin, C.; Firsching, R.; Schneider, T., Cytotoxic effect of different statins and thiazolidinediones on malignant glioma cells. *Cancer Chemother. Pharmacol.* **2011,** *67* (5), 1193-1201.
72. Carlsson, S. K.; Brothers, S. P.; Wahlestedt, C., Emerging treatment strategies for glioblastoma multiforme. *EMBO Mol. Med.* **2014,** *6* (11), 1359-1370.
73. Huse, J. T.; Holland, E. C., Targeting brain cancer: advances in the molecular pathology of malignant glioma and medulloblastoma. *Nat. Rev. Cancer* **2010,** *10*, 319.
74. Di Tomaso, E.; Pang, J. C. S.; Ng, H. K.; Lam, P. Y. P.; Tian, X. X.; Suen, K. W.; Hui, A. B. Y.; Hjelm, N. M., Establishment and characterization of a human cell line from paediatric cerebellar glioblastoma multiforme. *Neuropathol. Appl. Neurobiol.* **2000,** *26* (1), 22-30.
75. Schulze, M.; Fedorchenko, O.; Zink, T. G.; Knobbe-Thomsen, C. B.; Kraus, S.; Schwinn, S.; Beilhack, A.; Reifenberger, G.; Monoranu, C. M.; Sirén, A. L.; Jeanclos, E.; Gohla, A., Chronophin is a glial tumor modifier involved in the regulation of glioblastoma growth and invasiveness. *Oncogene* **2015,** *35*, 3163.
76. Lin, R.-Z.; Chang, H.-Y., Recent advances in three-dimensional multicellular spheroid culture for biomedical research. *Biotechnol. J.* **2008,** *3* (9-10), 1172-1184.
77. Netti, P. A.; Berk, D. A.; Swartz, M. A.; Grodzinsky, A. J.; Jain, R. K., Role of Extracellular Matrix Assembly in Interstitial Transport in Solid Tumors. *Cancer Res.* **2000,** *60*, 2497-2503.
78. Goodman, T. T.; Olive, P. L.; Pun, S. H., Increased nanoparticle penetration in collagenase treated multcellular spheroids. *Int. J. Nanomed.* **2007,** *2* (2), 265-274.
79. Solomon, M. A.; Lemera, J.; D'Souza, G. G. M., Development of an in vitro tumor spheroid culture model amenable to high-throughput testing of potential anticancer nanotherapeutics. *J. Liposome Res.* **2016,** *26* (3), 246-260.
80. Perrault, S. D.; Walkey, C.; Jennings, T.; Fischer, H. C.; Chan, W. C. W., Mediating Tumor Targeting Efficiency of Nanoparticles Through Design. *Nano Lett.* **2009,** *9* (5), 1909-1915.
81. Zinger, A.; Koren, L.; Adir, O.; Poley, M.; Alyan, M.; Yaari, Z.; Noor, N.; Krinsky, N.; Simon, A.; Gibori, H.; Krayem, M.; Mumblat, Y.; Kasten, S.; Ofir, S.; Fridman, E.; Milman, N.; Lübtow, M. M.; Liba, L.; Shklover, J.; Shainsky-Roitman, J.; Binenbaum, Y.; Hershkovitz, D.; Gil, Z.; Dvir, T.; Luxenhofer, R.; Satchi-Fainaro, R.; Schroeder, A., Collagenase Nanoparticles Enhance the Penetration of Drugs into Pancreatic Tumors. *ACS Nano* **2019,** *13* (10), 11008-11021.
82. Desoize, B.; Jardillier, J.-C., Multicellular resistance: a paradigm for clinical resistance? *Crit. Rev. Oncol. Hematol.* **2000,** *36* (2), 193-207.
83. Visvader, J. E.; Lindeman, G. J., Cancer stem cells in solid tumours: accumulating evidence and unresolved questions. *Nat. Rev. Cancer* **2008,** *8*, 755.
84. Lathia, J. D.; Mack, S. C.; Mulkearns-Hubert, E. E.; Valentim, C. L. L.; Rich, J. N., Cancer stem cells in glioblastoma. *Genes Dev.* **2015,** *29* (12), 1203-1217.
85. Rich, J. N., Cancer Stem Cells in Radiation Resistance. *Cancer Res.* **2007,** *67* (19), 8980.
86. Beier, D.; Schulz, J. B.; Beier, C. P., Chemoresistance of glioblastoma cancer stem cells - much more complex than expected. *Mol. Cancer* **2011,** *10* (1), 128.
87. Zhang, F.; Xu, C.-L.; Liu, C.-M., Drug delivery strategies to enhance the permeability of the blood-brain barrier for treatment of glioma. *Drug Des. Dev. Ther.* **2015,** *9*, 2089-2100.
88. Wolff, A.; Antfolk, M.; Brodin, B.; Tenje, M., In Vitro Blood–Brain Barrier Models—An Overview of Established Models and New Microfluidic Approaches. *J. Pharm. Sci.* **2015,** *104* (9), 2727-2746.
89. Avdeef, A.; Deli, M. A.; Neuhaus, W., In Vitro Assays for Assessing BBB Permeability. In *Blood-Brain Barrier in Drug Discovery*, John Wiley, 2015; pp 188-237.
90. Chacko, A. M.; Li, C.; Pryma, D. A.; Brem, S.; Coukos, G.; Muzykantov, V., Targeted delivery of antibody-based therapeutic and imaging agents to CNS tumors: crossing the blood-brain barrier divide. *Expert Opin. Drug Deliv.* **2013,** *10* (7), 907-26.
91. Thomas, A.; Ou-Yang, H. D.; Lowe-Krentz, L.; Muzykantov, V. R.; Liu, Y., Biomimetic channel modeling local vascular dynamics of pro-inflammatory endothelial changes. *Biomicrofluidics* **2016,** *10* (1), 014101.
92. Lippmann, E. S.; Azarin, S. M.; Kay, J. E.; Nessler, R. A.; Wilson, H. K.; Al-Ahmad, A.; Palecek, S. P.; Shusta, E. V., Derivation of blood-brain barrier endothelial cells from human pluripotent stem cells. *Nat. Biotechnol.* **2012,** *30*, 783.
93. Wang, Q.; Huang, C.-r.; Jiang, M.; Zhu, Y.-y.; Wang, J.; Chen, J.; Shi, J.-h., Binding interaction of atorvastatin with bovine serum albumin: Spectroscopic methods and molecular docking. *Spectrochim. Acta A* **2016,** *156*, 155-163.
94. He, Z.; Wan, X.; Schulz, A.; Bludau, H.; Dobrovolskaia, M. A.; Stern, S. T.; Montgomery, S. A.; Yuan, H.; Li, Z.; Alakhova, D.; Sokolsky, M.; Darr, D. B.; Perou, C. M.; Jordan, R.; Luxenhofer, R.; Kabanov, A. V., A high capacity polymeric micelle of paclitaxel: Implication of high dose drug therapy to safety and in vivo anti-cancer activity. *Biomaterials* **2016,** *101*, 296-309.
95. Lins, R. L.; Matthys, K. E.; Verpooten, G. A.; Peeters, P. C.; Dratwa, M.; Stolear, J. C.; Lameire, N. H., Pharmacokinetics of atorvastatin and its metabolites after single and multiple dosing in hypercholesterolaemic haemodialysis patients. *Nephrol. Dial. Transplant.* **2003,** *18* (5), 967-976.

TABLE OF CONTENTS graphic